27th Symposium on Naval Hydrodynamics
Seoul, Korea, 5-10 October 2008

Modeling of Free Surface Flows with Elastic Bodies Interactions

A. Souto-Iglesias[1], S.R. Idelsohn[2,3], J. Martí[4], R. Zamora-Rodríguez[1], E. Oñate[2]

[1] Technical University of Madrid (UPM), Madrid, Spain,
[2] International Centre for Numerical Methods in Engineering (CIMNE), Barcelona, Spain.
[3] National University of Littoral (UNL), Santa Fe, Argentina.
[4] International Centre for Computational Methods in Engineering (CIMEC)- UNL.

ABSTRACT

In this paper, a series of new fluid and structure interactions test cases with strong free surface effects are presented and computations of such flows with the Particle Finite Element Method (PFEM) (Idelsohn, Oñate, Del Pin and Calvo, 2006) are documented. The structures object of study are elastic cantilever bars clamped inside sloshing tanks subjected ro roll motion. The possibilities of PFEM for the coupled simulation of moderately violent free surface flows interacting with elastic bodies are investigated. The problem can be described as the coupling of a sloshing flow with an easily deformable elastic body. A series of experiments designed and executed specifically for these tests are also described. The experiments comprise cases with different liquid height and liquids of different viscosity. The aim is to identify canonical benchmark problems in FSI (Fluid and Structure Interactions), including free surfaces, for future comparisons between different numerical approaches.

INTRODUCTION

The availability of sufficient computer power, together with the maturity of the tools for CFD analysis, open the way to the simulation of flow problems of increasing complexity. Between the many potential applications, the simulation of FSI problems including free-surface flows represents a particularly interesting case. The challenge is in this case connected both to the inherent difficulty to solve FSI problems with the simulation of a highly unsteady flow with a rapid variation of the fluid domain.

There are in the literature abundant comparisons between experiments and numerical solutions for FSI problems without free surfaces. Publications concerning the comparison between experimental data and results computed with different numerical techniques for pure fluid mechanics problems with free surface flows are also available. Nevertheless, the combined case in which the fluid flow including the free surface motion interacts with elastic structures has not been well documented and it is difficult to find experimental results with which to compare the simulations in order to check their accuracy.

The objective of this work is to present a series of three examples for FSI problems for which the presence of free surfaces is a significant factor in the types of flows that can be found. The examples fall in the range of sloshing type problems, for which previous works have been done by the authors, using other numerical techniques (Souto-Iglesias, Delorme, Pérez-Rojas and Abril-Pérez, 2006) .

From the numerical point of view, different methods have been devised over the last years to deal with this challenge. In this work, only a comparison with the Particle Finite Element Method (PFEM) will be performed. A complete description of PFEM may be found in (Idelsohn, Oñate and Del Pin, 2004) . Only a light overview of this numerical method will be described in the next section for the sake of completeness.

A comprehensive comparison of the PFEM method with experimental results including mesh refinement and convergence test can be found in (Larese, Rossi, Oñate and Idelsohn, in press). In this reference only fluid flow problems with no interaction with elastic structures are discussed. The extension to deal with the elastic deformation of an structure in a fluid is the objective of this work.

Experimentation dealing with sloshing flows has been been a field mainly leaded by classification soci-

eties like DNV, ABS or LRS (Rognebakke, Hoff, Allers, Berget, Berge and Zhao, 2005), with some exceptions like Akyildiz and Erdem (2005), who studied the pressure distribution in a sloshing tank during roll motion. Nevertheless, not much experimental work on combined sloshing flows and elastic bodies can be found apart from specific studies dealing mainly with dam-breaking and breakwaters problems (Antoci, Gallati and Sibilla, 2007). The very few existing studies correspond to Reynolds numbers regimes difficult to reproduce numerically due to the onset of turbulence. Therefore, the authors believe the present paper has quite ample possibilities as validation information for fluid-structure interaction simulation codes because experimental data corresponding to lower Reynolds numbers are provided. For these regimes, the numerical results do not present resolution problems because turbulence does not appear or it is very limited. Also, having elastic bodies implies bigger deformations thus reducing experimental uncertainties. Engineering applications of such sloshing flows are for instance the design of the pump-towers inside the LNG tanks. These bodies are subjected to extreme fluid loads during the sloshing events (Rognebakke, Hoff, Allers, Berget, Berge and Zhao, 2005). Other interesting application of these problems is the FSI inside safety valves for pressure reduction, where an elastic plate deforms owing to water pressure, allowing part of the fluid to flow out at atmospheric conditions, thus causing a pressure relief in the connected pipe (Antoci, Gallati and Sibilla, 2007).

Extremely interesting experimental work in a related FSI field was carried out in the sixties by Lindholm, Kana, Chu and Abramson (1965) . They conducted tests with steel cantilever plates clamped to a rigid I-beam support structure and partially submerged in water. They devised a series of corrections to linear beam and thin-plate theories to account for the plate aspect and thickness ratios. They also included apparent mass factors derived from hydrodynamic strip theory. Finally, and most interestingly, they studied the influence of the plates being partially submerged on their resonance frequencies. Lindholm, Kana, Chu and Abramson (1965) work is so crucial that it has been used as experimental reference for the most recent modeling papers (Ergin, A., Ugurlu 2003), (Kara and Vassalos 2007), (Liang, Liao, Tai and Lai, 2001) on hydroelasticity problems.

Nevertheless, when studying a cantilever plate partially immersed in a liquid with a free surface, not only its mechanical behavior should be addressed but also the type of free surface flow that can be found in the fluid. Therefore, the experimental results should cover also the fluid dynamics part of the problem and it is desirable that the deformations in the body are non negligible in order to make the case useful for validating a range of numerical codes as well as for reducing relatives experimental uncertainties. Actually, there is at the moment an increasing interest to model and simulate fluid and structure interactions in which the deformation rates of both the fluid and the body are of the same order of magnitude as well as the motion characteristic scales. Good examples of such attempts can be found in Idelsohn, Martí, Limache and Oñate (2008) and Walhorn, Kölke, Hübner and Dinkler (2005), in which a dam-breaking impact on an elastic cantilever is simulated.

In order to perform experiments in which deformations are high under not extreme fluid loads, elastic bodies with Young's Modulus of the order of 10^6 are necessary. Also, since the computations are very time consuming, a pure two-dimensional experimental case would be desirable. Apart from the experiments of Antoci, Gallati and Sibilla (2007), more focused on the simulations than in the completeness of the experimental work, no such characteristics empirical tests can be found in the literature. In order to fill this gap a set of experiments clamping an elastic body both to the roof top as well as to the bottom of a rectangular tank subjected to roll motion have been performed. The length of the body, the liquid, the roll frequency and other parameters are varied. Both the shape of the free surface as well as the mode decomposition of the probe deflected shape are discussed.

NUMERICAL SIMULATION

Different methods have been devised over the years to deal with transient free surface problems. A first category of algorithms is based on the idea of tracking the evolution of a free surface defined with the help of a smooth distance function (Level Set)(Osher and Fedkiw, 2001) , or of a scalar value representing the quantity of fluid in a given area. This is the basis of the Volume of Fluid (VOF) technique. This scalar function is convected according to the flow velocity field once a suitable discretization of the space is provided. This philosophy interacts quite nicely with existing Eulerian codes thus justifying the success of the VOF method in the CFD community. The VOF formulation is able to compute the separation (or reattachment) of parts of the fluid domain; nevertheless some concerns remain particularly related with the imposition of the Dirichlet boundary conditions on the free surface. Even if all the advantages of Eulerian methods on fixed meshes can be retained, the VOF approach tends to introduce some diffusion in the position of sharp interfaces (see for example Zalesak's circle benchmark in Osher and Fedkiw (2006)).

An alternative formulation, known as Smooth Par-

ticle Hydrodynamics (SPH), allows a Lagrangian simulation of a number of particles through the use of a simple meshless technology (Roubtsova and Kahawita, 2006), (Antoci, Gallati and Sibilla, 2007). This technique, which is raising an increasing interest in the scientific community due to its simplicity and computational efficiency, faces however some severe drawbacks. First it has troubles in representing constant functions (it is not a partition of unity) which implies problems in proving the convergence. Secondly its application is appealing as long as an explicit formulation for the fluid can be used, which makes it unattractive for truly incompressible flows (Bonet, Kulasagaram, Rodriguez-Paz and Profit, 2004). It has also the drawbacks of the difficulties to perform dynamic refinement which means it is very difficult to resolve boundary layers. This technique has been, as already mentioned, used by Antoci, Gallati and Sibilla (2007) to simulate the coupling of a dam-break with an elastic curtain, providing as well experimental data for water, with which the numerical results are compared in terms of displacements of the solid body and liquid levels at specific locations.

The possibility exists to blend the advantages of "Particle" methods with finite element (FE) methods. The Particle Finite Element Method (PFEM from now on) achieves this result by convecting in a Lagrangian way the fluid "particles" while redefining at the beginning of each step a new mesh. This allows to reproduce very accurately the convection of the nodes and to impose Dirichlet conditions in a natural way. Further, all the convergence results can be inherited from the FEM which guarantees the reliability and good convergence properties of the computational predictions (Idelsohn, Oñate and Del Pin, 2004) .

The PFEM treats the mesh nodes in the fluid domain as particles which can freely move and even separate from the main fluid domain representing, for instance, the effect of water drops. A finite element mesh connects the nodes defining the discretized domain where the governing equations are solved in the standard FEM fashion. The PFEM is the natural evolution of recent work of the authors for the solution of FSI problems using Lagrangian finite element and meshless methods (Idelsohn, Oñate and Del Pin, 2004) , (Oñate, Idelsohn, Del Pin and Aubry, 2004) .

An obvious advantage of the Lagrangian formulation is that the convective terms disappear from the fluid equations. The difficulty is however transferred to the problem of adequately (and efficiently) moving the mesh nodes. We use innovative mesh regeneration procedure blending elements of different shapes using an extended Delaunay tesselation (Idelsohn, Oñate, Calvo and Del Pin, 2003), (Idelsohn, Calvo and Oñate, 2003).

The need to properly treat the incompressibility condition in the fluid still remains in the Lagrangian formulation. The use of standard finite element interpolations may lead to a volumetric locking defect unless some precautions are taken (Donea and Huerta, 1998) , (Zienkiewicz, Taylor and Nitharasu, 2005) . In our work the stabilization via a finite calculus (FIC) procedure has been chosen (Oñate, 2000) . Applications of the FIC method for incompressible flow analysis using linear triangles and tetrahedral meshes have been reported in (Oñate, Idelsohn, Del Pin and Aubry, 2004) and Oñate and Idelsohn (1998).

OVERVIEW OF THE PARTICLE FINITE ELEMENT METHODS (PFEM)

Let us consider a domain containing both a fluid and a solid body sub domains. The moving particles interact with the solid boundaries thereby inducing the deformation of the solid which in turn affects the flow motion making the problem a fully coupled one. In the PFEM method, both the fluid and the solid domains are modeled using an updated Lagrangian formulation. This means that all the variables in the fluid and solid domains are assumed to be known at time t. The finite element method (FEM) is used to solve the continuum equations in both domains.

A mesh discretizing these domains must be generated in order to solve the governing equations for both the fluid and solid problems in the standard FEM fashion.

We note that the nodes discretizing the fluid and solid domains are viewed as material particles whose motion is tracked during the transient solution. This is useful to model the separation of fluid particles from the main fluid domain and to follow their subsequent motion as individual particles with a known density, initial acceleration and velocity and subjected to gravity forces. It is important to note that each particle is a material point characterized by the density of the solid or fluid domain to which it belongs. The mass of a given domain is obtained by integrating the density at the different material points over the domain. The quality of the numerical solution depends on the discretization chosen, as in the standard FEM.

Adaptive mesh refinement techniques can be used to improve the solution in zones where large gradients of the fluid or the structure motion description fields occur. For clarity purposes we will define the collection or cloud of nodes (C) pertaining to the fluid and solid domains, the volume (V) defining the analysis domain for the fluid and the solid and the mesh (M) than is used for the discretization of both domains (fig. 1). The process of calculation is then as follows:

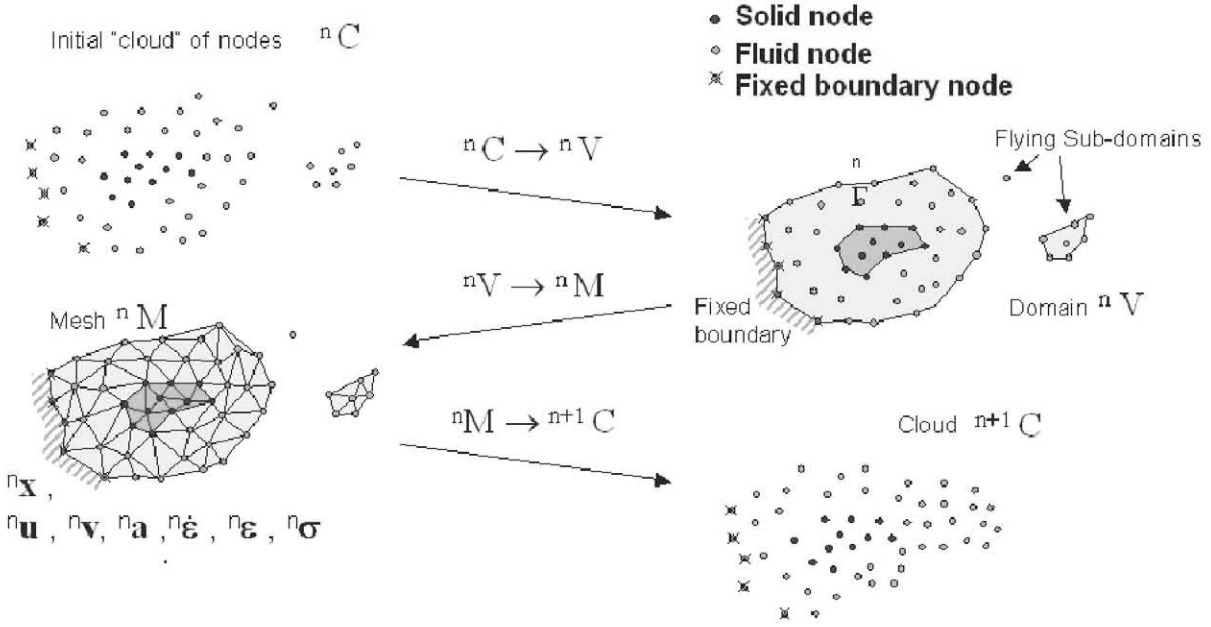

FIGURE 1: Sequence of steps to update a "cloud" of nodes from time n($t = t_n$) to time $n + 1(t = t_{n+\Delta t})$

1. The starting point at each time step is the cloud of points with which the fluid and solid domains are represented. C denotes the cloud at time $t = t_n$ (fig. 1).

2. The boundaries for both the fluid and solid domains defining the analysis domain V in the fluid and the solid phases have then to be identified. This is an essential step as some boundaries (such as the free surface in fluids) may be severely distorted during the solution process including separation and re-entering of nodes. The Alpha Shape method (Edelsbruner and Mucke, 1994) is used for the boundary definition.

3. Discretize the fluid and solid domains with a finite element mesh M. In our work we use an innovative mesh generation scheme based on the extended Delaunay tessellation (Idelsohn, Calvo and Oñate, 2003).

4. Solve the coupled Lagrangian equations of motion for the fluid and the solid domains. Compute the relevant state variables in both domains at the next (updated) configuration for $t + \Delta t$: velocities, pressure and viscous stresses in the fluid and displacements, stresses and strains in the solid.

5. Move the mesh nodes to a new position C^{n+1} where $n + 1$ denotes the time $t_n + \Delta t$, in terms of the time increment size. This step is typically a consequence of the solution process of step 4.

6. Go back to step 1 and repeat the solution process for the next time step.

FIGURE 2: Tank testing device

EXPERIMENTAL MODEL

The experimental data used for the comparison have been obtained with laboratory tests carried out specif-

ically for this study, using the tank testing facilities at UPM. The experimental equipment is represented in figure 2. It is composed of a structure that holds the tank and an electrical engine that produces a harmonic rolling motion on the moving part of the structure, which embraces a tank with the liquid inside. The system incorporates a high precision torquemeter with a 200 Nm range because it is routinely used for the design of the passive anti-roll tanks for fishing vessels. It has been used previously aimed at providing validation data for CFD studies, both in terms of free surface shape as well as in terms of the effect of the liquid with respect to the tank motion, by measuring the torque produced by the motion of the liquid (Souto-Iglesias, Delorme, Pérez-Rojas and Abril-Pérez, 2006) as well as the wave impact pressures (Delorme, Roca-Fernández-Vizarra, Souto-Iglesias and González-Gutiérrez, 2007). In figure 3 an image corresponding to a sloshing experiment performed with the same system, corresponding to a campaign for studying the the value of the pressure peaks during the wave impacting events on tank roofs is presented.

FIGURE 3: Sloshing experiment

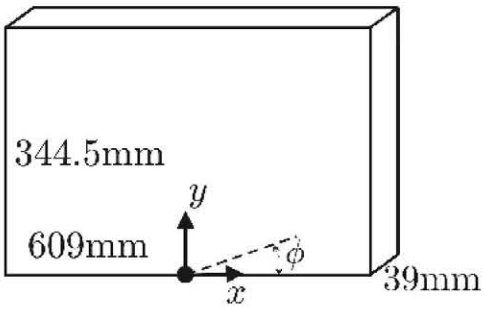

FIGURE 4: Tank dimensions. Rolling angle ϕ. Axis

The tank, with which the experiments of the present study have been performed is a prismatic one, made of methacrylate. Their main dimensions are a length of 609.0mm, a height of 344.5mm and a width of 39.0mm (figure 4). The is for to move in an oscillatory way around a fixed point in order to produce the waves. In this study the rotation center is the center of the bottom of the tank. The magnitude of maximum angle as well as the angular can be regulated, aimed at matching the critical sloshing frequencies for different liquid levels. The container is closed in the upper wall, but two holes were made on the top in order to let the air circulate freely without affecting the liquid and the solid body behavior.

On the bottom wall or in the upper one, an elastic beam may be clamped to interact with the incompressible fluid. The beams used have a thickness of 4 mm and a width of 33.2 mm which is enough to simulate a 2D flow without touching the lateral walls. The minimum admissible gap was found to be 2.9 mm for the longest configuration of the probes (287.1 mm). It would be desirable to have a smaller gap with the tank walls but due to the flexibility of the material, the rubber beam is prone to slightly bend on the front direction driven by capillarity and surface tension effects, thus touching the tank walls and invalidating the experiment. On top of this, it was discovered that smaller gaps made it extremely difficult the positioning of the clamp anchorage. Another rubber band with a wider gap was also tested in the same conditions (fig. 6) and for every experiment the bands were placed in both symmetric configurations, to find no significant variations in the body displacements. An image of the fitting of the rubber inside the tank can be found in figure 7.

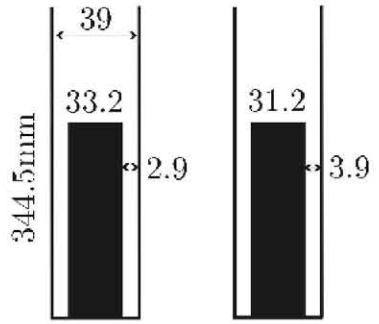

FIGURE 6: Rubber bands drafts (not to scale)

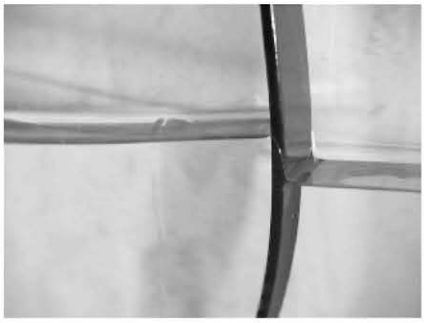

FIGURE 7: Rubber band inside the tank

The material for the probes clamped to the bottom is a dielectric polyurethane resin, whose trademark is AX-

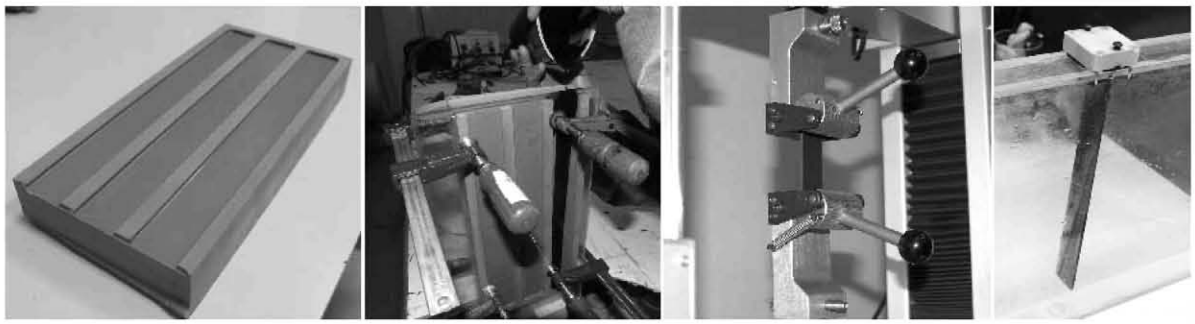

FIGURE 5: Mould for the probes, synthesizing process, traction test and anchorage

SON RE 11820-(9). It was specifically syntethized for these tests by mixing the components and carefully filling a mould milled with the probe dimensions (fig. 5). The density of the probes was established as 1.1 gr/cm^3. The Young modulus (initial slope), measured with a traction test is approximately 0.006 GPa. A spare probe was manufactured to be used for the traction destructive tests (fig. 5). An important aspect to be taken into account is that the mechanical properties of this material are not affected by its immersion in the liquids during the sloshing tests. For the probes clamped to the top, a commercial neoprene rubber was used. Its density is 1.9 gr/cm^3 and its Young modulus is 0.004 GPa.

An anchorage piece was designed and milled to clamp the probe to the tank roof or bottom guaranteeing both a very good bending restriction at the base, as well as an accurate leveling of the piece at the bottom/top of the tank(see fig. 5). In this way, the flow is not significantly affected on the vicinity of the probe by the anchorage. A hole was prepared in the tank to receive the anchorage piece.

Regarding the liquids, fresh water and a commercial sunflower oil were used. The temperature of the tests was 23 °C. The sunflower oil density was 0.917. The kinematic viscosity of the sunflower oil was measured using a Canon-Fenske viscosimeter running a series of tests at 23 °C, 40 °C and at 50 °C and by extrapolating the tabulated constants for the viscosimeter that corresponded to the latter temperatures. At 23 °C its value is 50 cst (5e-5 m^2/s). This means that the Reynolds number of the tests will be in principle 50 times lower for the sunflower oil when compared with the water case. The liquid levels considered were the same as the probe lengths, which implies that for all the probes there are two cases, one hanging, and the other clamped at the bottom, with the bar tip just at the free surface a rest. This is a limit case worth studying.

A computer program was implemented aimed at measuring the total displacement of the elastic beam at different heights. The program facilitates the analysis of the individual frames obtained from a conventional 25 FPS video register of the experiment. For the short beam cases, only the displacement of the end-point of the cantilever was measured. For the cases with a long beam, where several bending modes appear, displacements have been measured at several points marked on the beam front.

There seem to be several uncertainties to be bound in this experiment. They have their origin on the gap effect in terms of the two-dimensionality of the case. Measurement of the displacement means around 2mm uncertainty. Dimensioning the solid body is also not trivial due to its flexibility. It is not completely stable in its long configuration due to own weight, etc. For the moment all these considerations have been discarded, waiting for an ampler experimental campaign focused on addressing these and other issues.

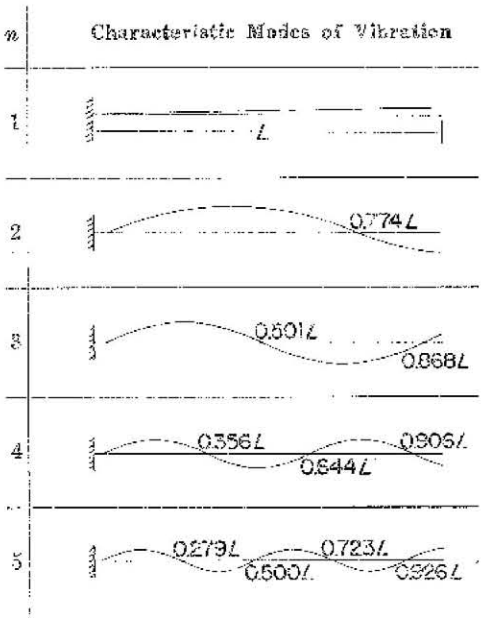

FIGURE 8: One end fixed and the other free vibration modes, from Volterra and Zachmanoglou (1965).

DEFLECTED BARS ANALYSIS

In their essential book, Volterra and Zachmanoglou (1965)(chapter 4.5) discussed the free transverse vibration of uniform continuos bars under various end conditions. They treated the most relevant cases starting with a bar with both ends simply supported. A very interesting physical and mathematical treatment of the equations allowed them to obtain the characteristic modes of vibration of the bar under those end conditions.

They extended the discussion to the case of one end fixed (clamped) and one end free, which is the one we are interested in. For this case, the characteristic modes of vibration are given by equation 2, in which L is the bar length, and the values of $k_n L$ (wavelengths of the modes) as well as the modes shapes can be seen in figure 8, taken from (Volterra and Zachmanoglou, 1965).

$$\begin{aligned} X_n(x) &= \{\cosh(k_n x) - \cos(k_n x) \\ &- \frac{\cos(k_n L) + \cosh(k_n L)}{\sin(k_n L) + \sinh(k_n L)} [\sinh(k_n x) - \sin(k_n x)]\Big\} \end{aligned} \quad (1)$$

The time history of the lateral displacement $w(\mathrm{x}, t)$ in a free vibration process can be expressed as in equation 2, in which the coefficients A_n and B_n are a function of the initial conditions and of the characteristic modes functions. They are found with a projection scheme, with the inner product 4, for which the characteristic modes are orthogonal functions.

$$w(\mathrm{x}, t) = \sum_n X_n(\mathrm{x}) f_n(t) \quad (2)$$

$$f_n(t) = A_n \cos(\hat{\omega}_n t) + B_n \sin(\hat{\omega}_n t) \quad (3)$$

$$\langle u, v \rangle := \int_0^L u(\mathrm{x}) v(\mathrm{x}) d\mathrm{x} \quad (4)$$

Each frequency $\hat{\omega}_n$ depends of the mode n wavelength as well as of the mechanical characteristics of the bar (Volterra and Zachmanoglou, 1965).

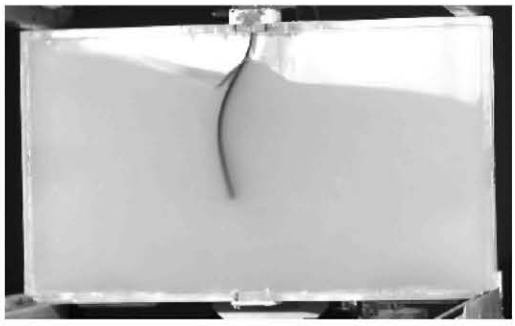

FIGURE 9: Several modes deformation

The analysis can be extended to forced vibrations by lateral forces, like the ones produced by the fluid on the bar in the experiments described in the paper. In this case, the time factors of equation 2 are not harmonic. Moreover, in our case, the influence of the bar on the flow field is big enough to induce very significant effects on those lateral forces. Therefore, we have a coupling effect between the velocity and pressure fields of the fluid and the bar motion, very difficult to model with a CFD code.

Since the characteristic modes are orthogonal with respect to the inner product 4, it would interesting to analyze the shape of the bar during the motion and check whether more modes than the first are excited by the fluid motion. In order to do so, the bar shape is digitized at different time steps and projected with the inner product 4 onto the function basis defined by the characteristic modes. Unfortunately no such analysis has been done in time to be included in this study, but it is worth thinking deeper about it because, clearly, higher modes are relevant in the motion as can be seen in figure 9.

EXPERIMENTAL VERSUS NUMERICAL COMPARISONS

Clamped elastic beam immersed in a shallow oil

The first two examples consist in a clamped beam of different lengths immersed in sunflower oil. Figure 10 represents the geometry of the first example and 11 the roll angle. The bar length is exactly the same as the liquid depth. This corresponds to a shallow depth case as will be now discussed.

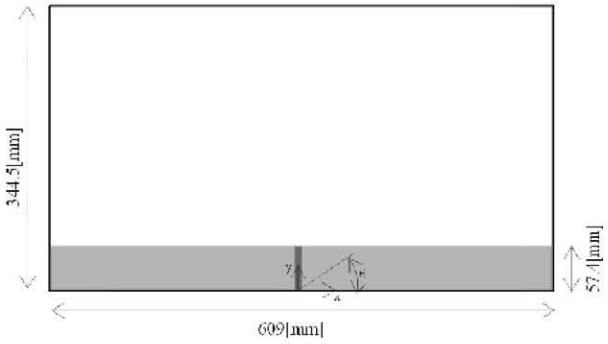

FIGURE 10: Clamped elastic beam in shallow oil setup

The simplest mean to characterize shallow depth sloshing flows is to resort to the dispersion relation for gravity waves in limited depth areas (Lamb, 1932).

$$\omega^2 = g\, k\, \tanh(k\, H) \quad (5)$$

In this expression, g is the gravitational acceleration, H the liquid level, ω is often called the sloshing frequency and k its corresponding wave number. The free surface

height function in a two dimensional rectangular container partially filled with liquid can be decomposed in a Fourier series with infinite wave numbers $k_n = n\pi/L$ where L is the tank breadth. If we focus on the first mode, the hyperbolic tangent argument of equation 5 becomes a factor of the ratio H/L. If the depth is great, then the tangent tends to one. If the ratio is for instance 1, the tangent value is 0.996 and therefore the effect of the depth on the waves will be very small. In this first case, the liquid depth is 57.4mm, with L being 609mm. The hyperbolic tangent factor is 0.29 which means that this is clearly a shallow water case. The first sloshing frequency, the one corresponding to the first mode will be noted w_1, and its corresponding period will be noted as T_1, being for this case 1.65s. The tank is excited with a 4 degrees amplitude roll motion whose frequency is T_1.

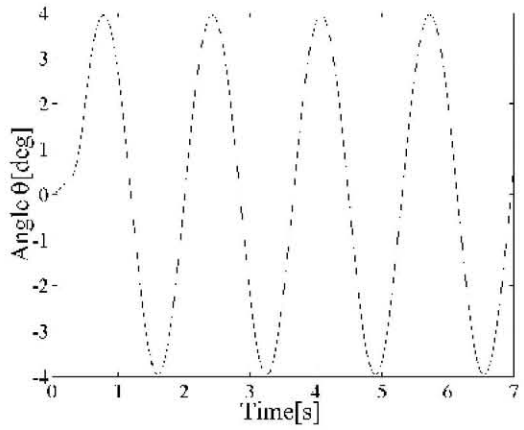

FIGURE 11: Clamped elastic beam in shallow oil: roll angle versus time

It is interesting to notice the ramp during the first instants of the motion(fig. 11). If pure harmonic motion is imposed during the simulations, this will translate into a lag with respect to the real motion. This is the reason for providing the real roll-angle history.

The numerical model has 15480 fluid particles and a total of 16939 nodes including the solid and the fluid part. The average time step used was equal to 0.0025s. Snapshots of different instances of the experiment are shown and compared with the PFEM results at the same times in fig. 14. The first frame, for $t = 0.92$ shows how PFEM is able to capture the hydraulic jump over the bar. Nevertheless, lack of resolution is appreciated in the last frame, for $t = 1.68$, for which the jump leaves a vacuum area which does not appear in the experiment.

For a more quantitative assessment of the agreement, we resort to figure 13 in which the x displacement corresponding to the end point of the beam has been represented for both the experiments and the PFEM solution. This displacement is measured in a local coordinate system of the tank, attached to the roll motion. In figure 12, an example of such measure is shown, corresponding to a negative x displacement. Figure 13 shows that the amplitude of the curve is well reproduced but there are small discrepancies that need further study. Also, for this case, the experimental displacements were very small thus implying bigger uncertainties in their values.

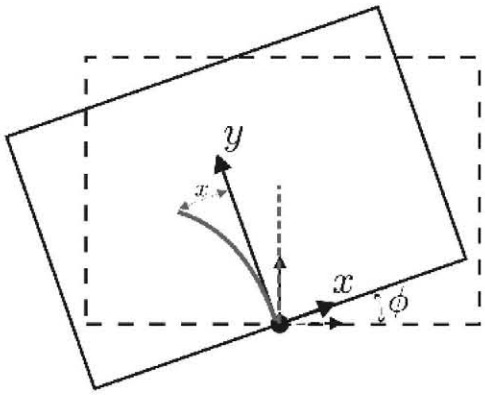

FIGURE 12: Local coordinate system for comparisons.

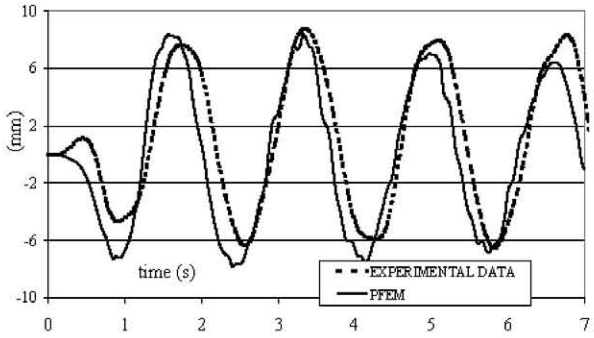

FIGURE 13: Clamped elastic beam in shallow oil: comparison of the displacement in X direction

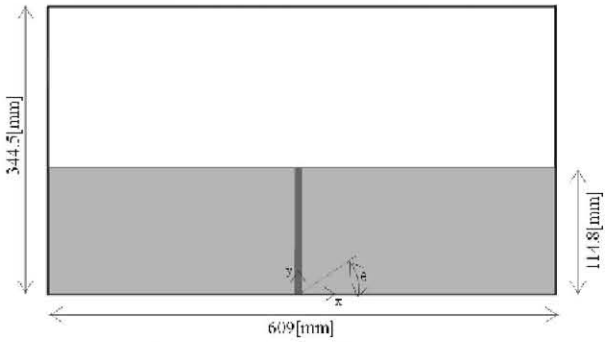

FIGURE 15: Clamped elastic beam immersed in mid-depth oil setup

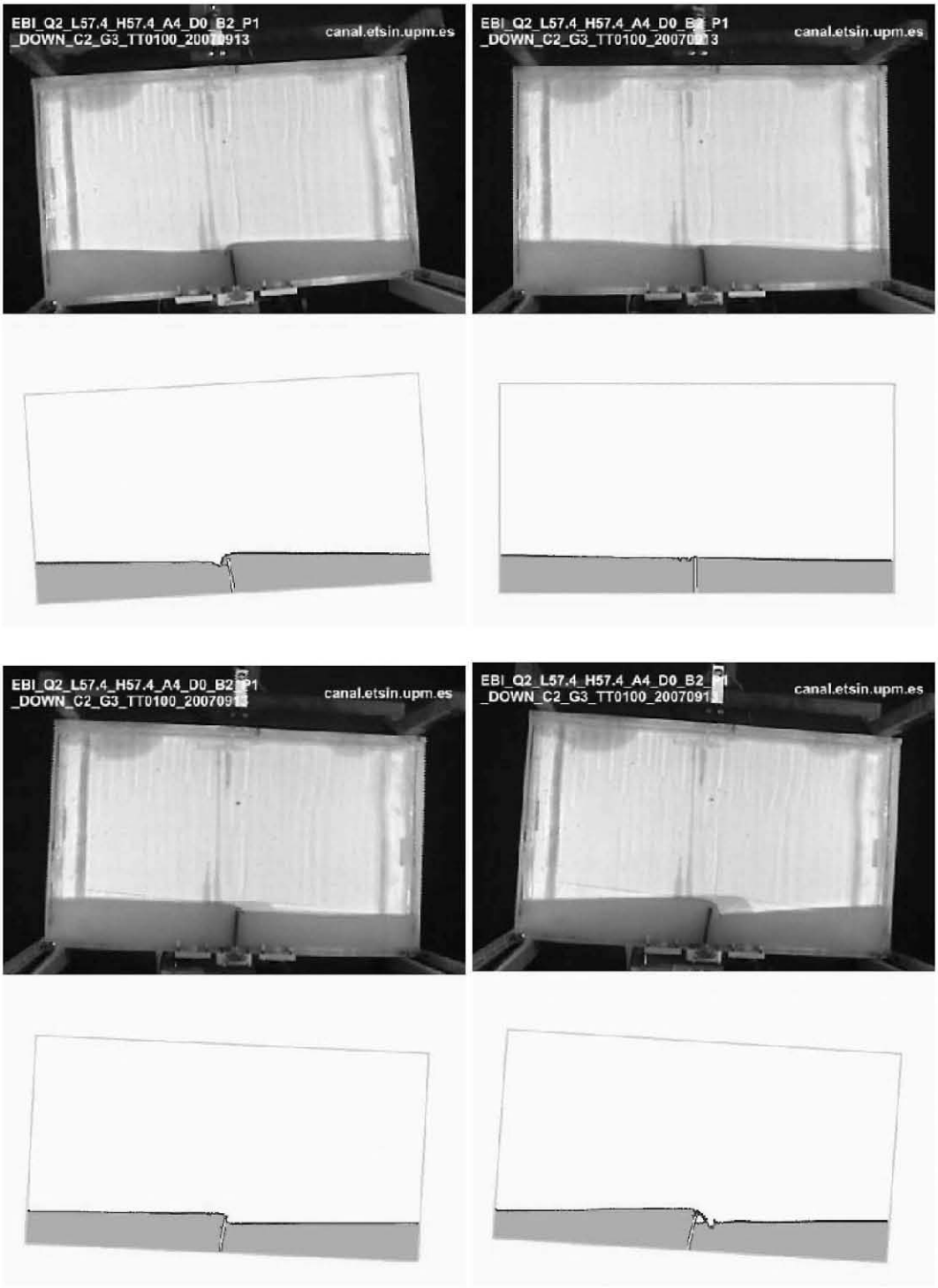

FIGURE 14: Clamped elastic beam in shallow oil: experimental versus numerical comparison for $t = \{0.92, 1.20, 1.40, 1.68\}[s]$

Clamped elastic beam immersed in mid-depth oil.

The second example is similar to the previous one but with twice the depth. The geometry and the motions of the container are shown in figures 15 and 16. The first sloshing period T_1 is in this case 1.21s and the forced roll amplitude is again 4 degrees. The PFEM mesh has a total of 16731 nodes with 15371 nodes corresponding to the liquid part.

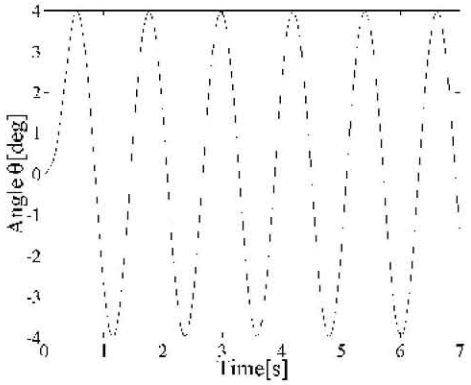

FIGURE 16: Clamped elastic beam immersed in mid-depth oil: roll angle

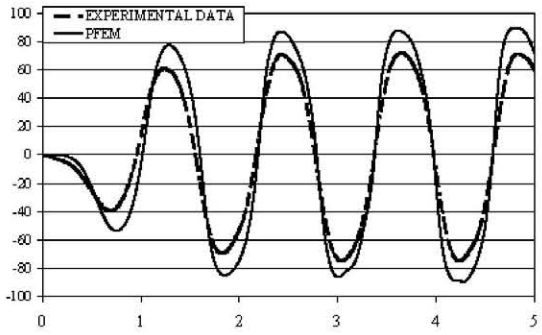

FIGURE 18: Clamped elastic beam immersed in mid-depth oil: comparison of the displacement in X direction

Figs. 17 and 18 show the free surface and the beam displacement of the end point at different time steps respectively. This is a complicated example in which the interaction between the fluid and the elastic beam is very strong. The x displacements have increased in one order of magnitude as can be seen by comparing the vertical scales in figures 13 and 18. The comparison of the numerical and experimental results is good in terms of the free surface shapes as well as in the bar end displacements, again with very good amplitudes and some dispersion that needs further study.

It is interesting to observe the shape of the free surface. The free surface deformations are much damped in comparison with the unbaffled tank, for which free surface patterns in the resonance cases are similar to those of figure 3.

Hanging elastic beam with shallow water

This is the most difficult example, with the beam hanging from the upper wall in such a fashion that the interaction with the fluid can be attained only due to the waves generated during the motion, otherwise having no interaction. The figures 19 and 20 show the initial geometry and the roll angle curve of the container whose maximum value was set to 2 degrees. The fundamental period is 1.65 because is the same liquid depth as in the first case (57.4mm). The number of particles used for the numerical solution was 16924 and time step was equal to 0.0025 s. Snapshots of the different instances of the experiment versus the PFEM results are shown in figure 21.

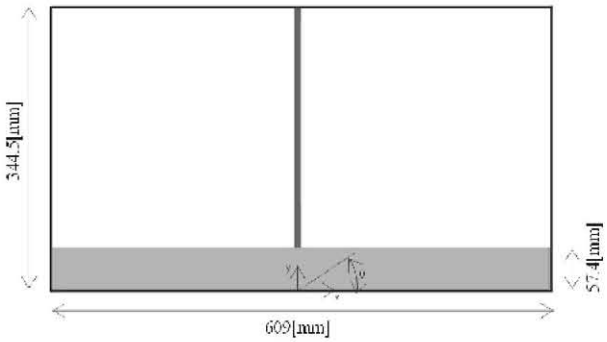

FIGURE 19: Hanging elastic beam with shallow water setup

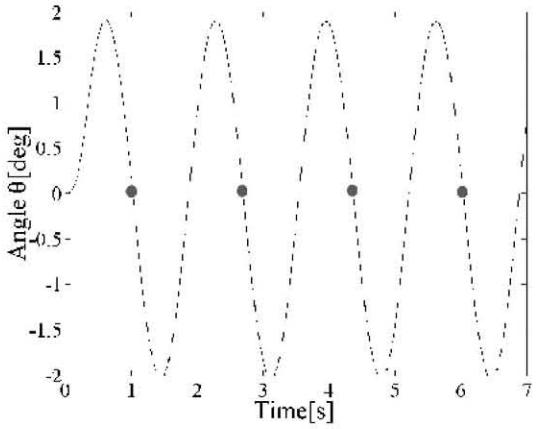

FIGURE 20: Hanging elastic beam with shallow water: roll angle versus time

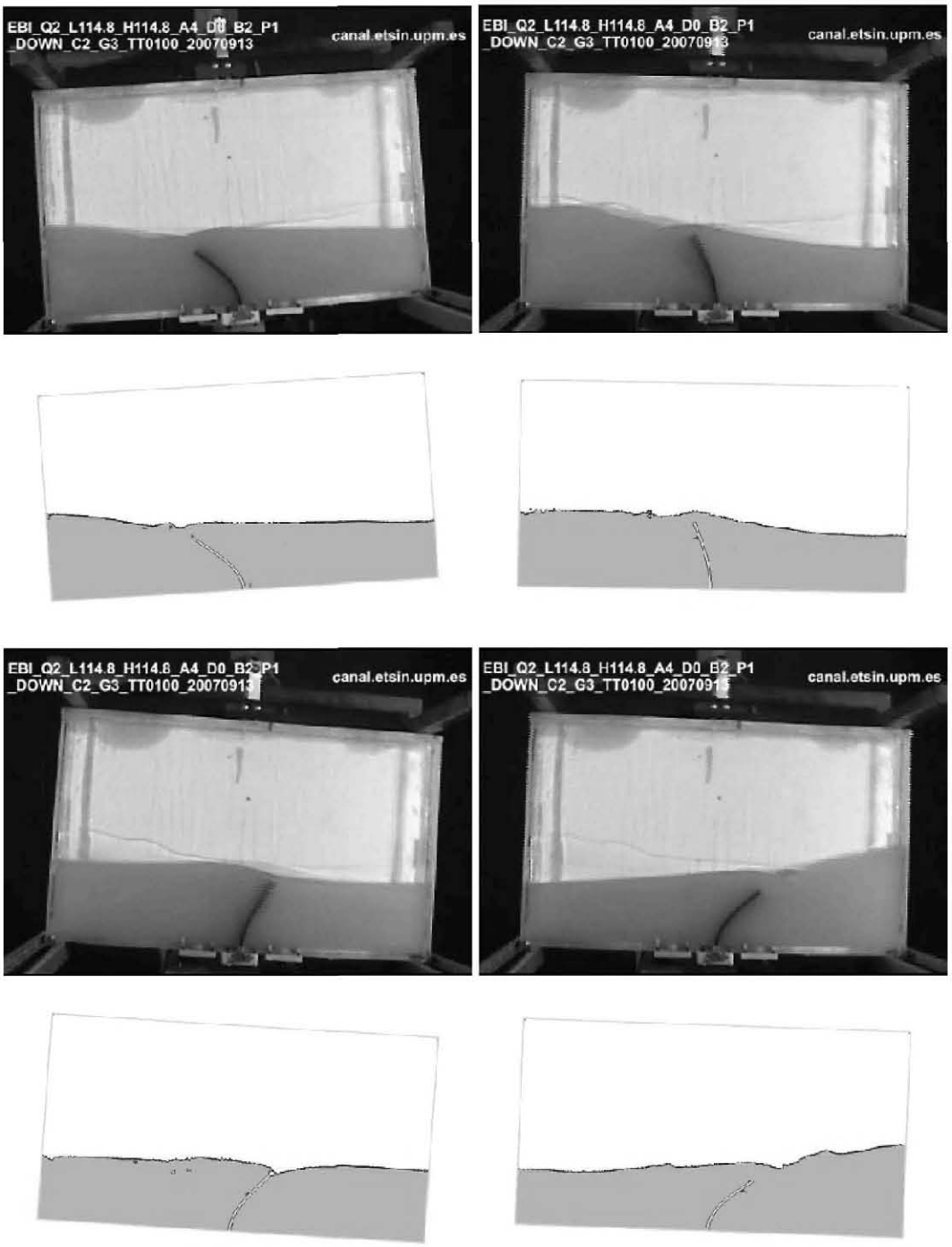

FIGURE 17: Clamped elastic beam in mid-depth oil: experimental versus numerical comparison $t = \{1.84, 2.12, 2.32, 2.56\}[s]$

In this example the natural frequency of the free surface wave does not coincide with the natural frequencies of the beam as a bending cantilever or as a pendulum. This produces a violent motion of the bar at time 2.96s (fig. 21) when the fluid structure interaction starts. Higher frequency motions of the elastic beam are induced at this moment, as can be appreciated on that frame, in which the interlacing problems of high speed motions recorded with conventional video cameras are clear. Both the free surface shape as well as the deformed bar shape are well reproduced even after more than three periods.

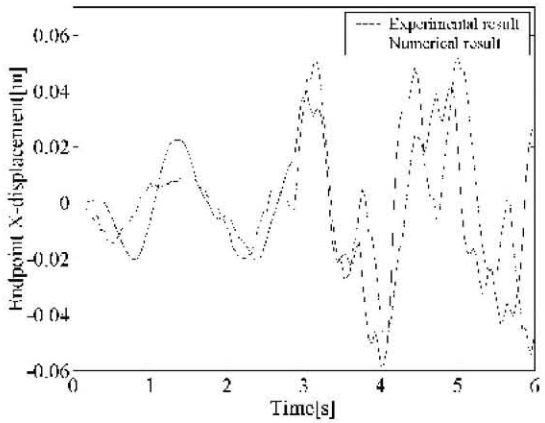

FIGURE 23: Hanging elastic beam in shallow water: comparison of the endpoint displacement in X direction

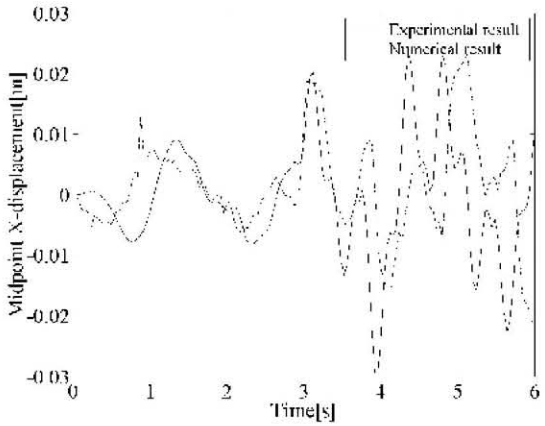

FIGURE 24: Hanging elastic beam in shallow water: comparison of the midpoint displacement in X direction

Figures 23 and 24 show the displacement of endpoint and midpoint of the beam as a function of time. The agreement between the numerical results and the experimental ones is good, taking in account the complexity of the example but further work has to be done. Other interesting figure is 25 in which the zero angle crossings instants marked in figure 20 are represented. As the motion builds up, the free surface becomes a bit steeper at each period. This is captured reasonably well by the simulations. The experimental frames come in this case not from a video register but from direct synchronized photographic pictures.

CONCLUSIONS AND FUTURE WORK

A series of new experimental tests have been presented in this paper aimed at providing data for the validation of FSI codes. The experiments have tried to document the interaction of confined sloshing flows with the deformations of elastic bars that interact with the free surface flows. The experiments show that the presence of the free surface is critical for some of the cases because on one hand the elastic body is a crucial factor in the wave amplitude response, and also the free surface waves can be crucial in the excitation of deformations in the bar for certain cases.

Numerical simulations have been performed using the Particle Finite Element Method (PFEM). PFEM is a powerful tool for solving free surface flow problems involving large deformation of the fluid domain. Good results have been obtained for the relevant parameters for the flow field and the elastic structure analyzed (such as the free surface and elastic beam position) as shown in the comparison with experimental data.

These new experiments suggest future work directions, both from the numerical and the experimental point of view. These can be summarized as:

1. Experimentally, it would be interesting to deeper analyze the two-dimensionality of the case studies by checking the deformations with broader containers and by providing more accurate data regarding the dependance of the deformed bar shapes and the bar gaps with the container walls.

2. Experimentally, it would be interesting to have PIV measurements of the velocity field. It seems a lot of vorticity is shed from the bar tips onto the flow.

3. Experimentally, as mentioned, it would be necessary to have error bounds to the different data, by performing a rigorous uncertainty analysis.

4. Numerically, it would be interesting to have detailed comparisons with other methods, like SPH, capable of simulating these problems. Actually, no convergence study has been provided in terms of the mesh resolution, neither comparisons in terms of the computation time with other numerical techniques.

5. Numerically, it would be interesting to study the vorticity fields as well as the influence of the

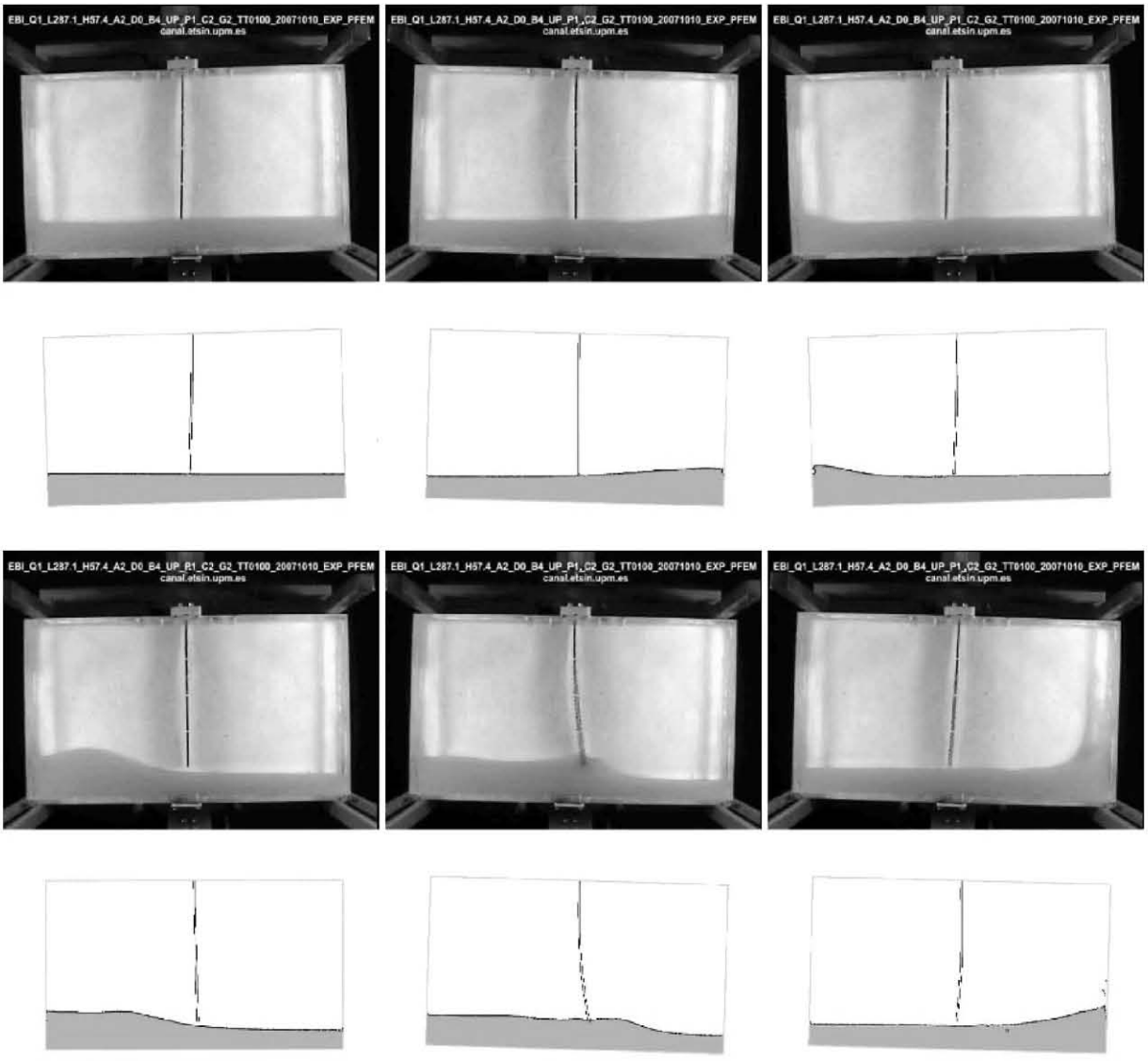

FIGURE 21: Hanging elastic beam in shallow water: experimental versus numerical comparison $t = \{0.76, 1.64, 2.4, 2.68, 2.96, 3.32, 3.4, 3.56, 3.80, 3.84, 4, 4.16\}[s]$

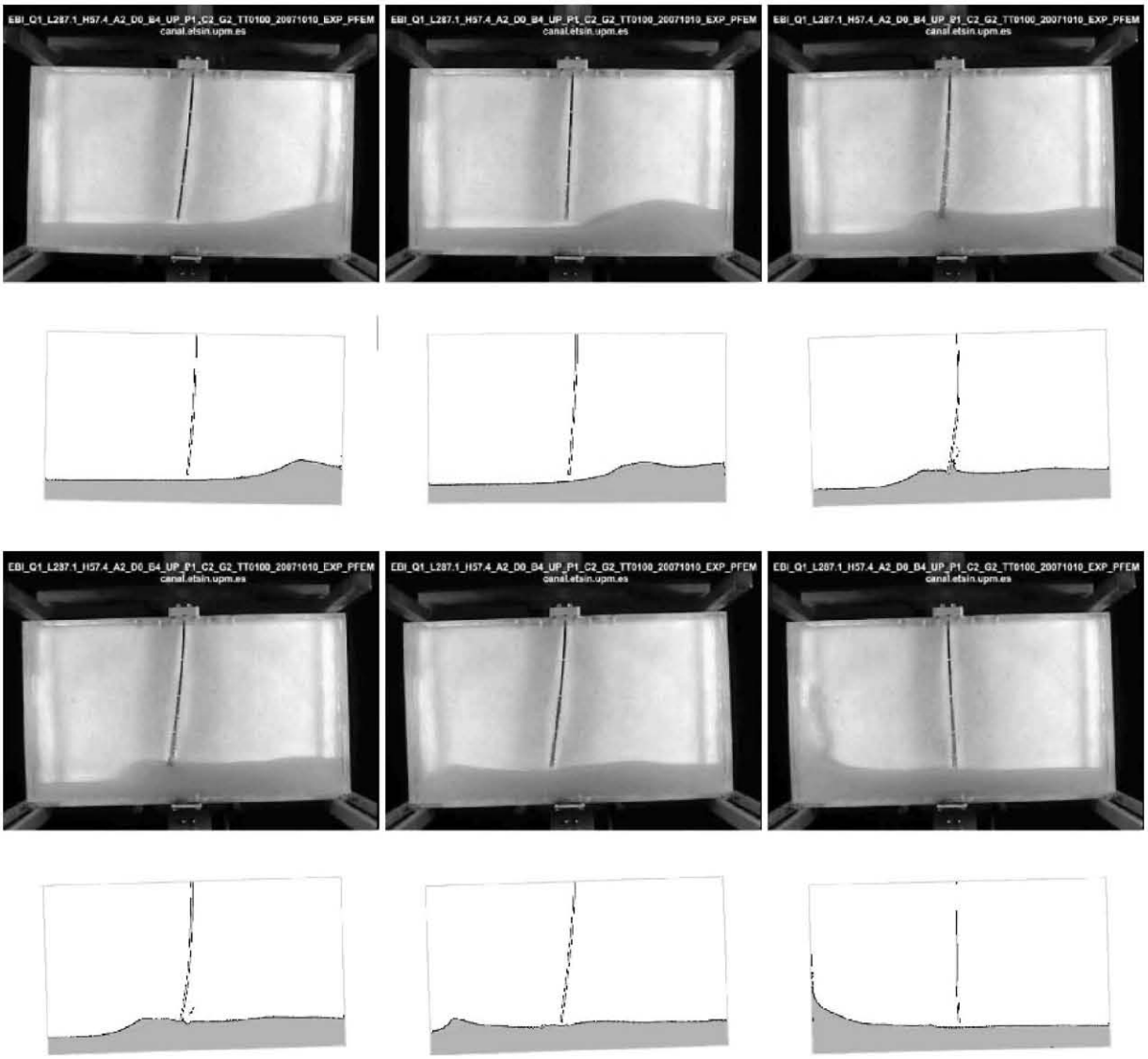

FIGURE 22: Cont.

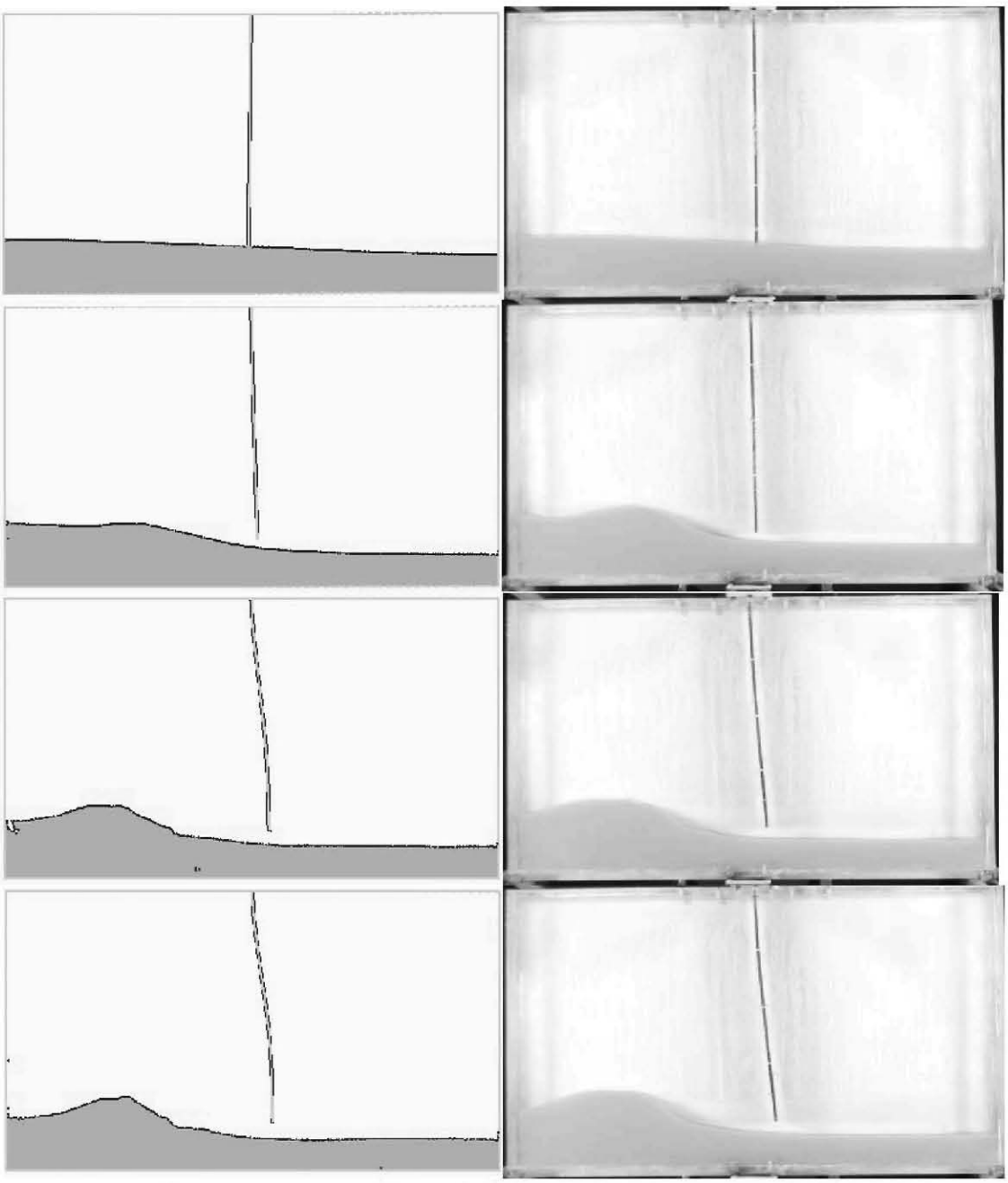

FIGURE 25: Zero crossings, approx. $0.5T_1$, $1.5T_1$, $2.5T_1$ and $3.5T_1$, as marked in figure 20

Reynolds numbers in some of the configurations. It seems turbulence is quite significant for some of the cases and this could partially justify the over damping in the experiments in the third test case, the hanging bar.

ACKNOWLEDGEMENTS

This work has been supported by the Alβan Programme of the European Union for High Level Scholarships for Latin America, scholarship No.E06D100984AR.

REFERENCES

Akyildiz, H., Erdem, Ü, "Experimental investigation of pressure distribution on a rectangular tank due to the liquid sloshing", Ocean Engineering, Vol. 32, 11-12, 2005, pp. 1503-1516.

Antoci, C., Gallati, M., Sibilla, S., "Numerical simulation of fluid-structure interaction by SPH" Computers & Structures Vol. 85, 2007, pp. 879-890.

Aubry, R., Idelsohn, S.R., Oñate, E., "Particle Finite Element Method in Fluid Mechanics including Thermal Convection-Diffusion", Computers and Structures, 83, 2005, pp. 1459-1475

Bonet, J., Kulasagaram, S., Rodriguez-Paz, M.X., Profit, M. "Variational formulation for the smooth particle hydrodynamics (SPH) simulation of fluid and solid problems´´. Computational Methods in Applied Mechanics and Engineering 193, 2004, pp. 1245-1256

Delorme, L., Roca-Fernández-Vizarra, P. , Souto-Iglesias, A., González-Gutiérrez, L., "Pressure Fields in LNG Tanks during Pitch Motions at Model Scale with SPH". 2nd International Conference on Computational Methods In Marine Engineering - MARINE 2007 Universidad Politécnica de Cataluña (UPC), Barcelona, Spain, June 2007.

Donea, J., Huerta, A., Finite Elements Methods for Flow Problems. Wiley, 2003.

Edelsbruner, H., Mucke, E.P., "Three dimensional alpha shape". ACM Transaction on Graphics, 13, 1994, pp. 43-72

Ergin, A., Ugurlu,B., "Linear vibration analysis of cantilever plates partially submerged in fluid", Journal of Fluids and Structures, Vol. 6, 17, 2003, pp. 927-939

Idelsohn, S.R., Martí, J., Limache, A., Oñate, E., "Unified Lagrangian formulation for elastic solids and incompressible fluids: Application to fluid-structure interaction problems via the PFEM", Computer Methods in Applied Mechanics and Engineering, Vol. 197, 19-20, 2008, pp. 1762-1776.

Idelsohn, S.R., Oñate, E., Del Pin, F., Calvo, N., "Fluid-Structure Interaction Using the Particle Finite Element Method". Computer Methods in Applied Mechanics and Engineering 195, 2006, pp. 2100-2123.

Idelsohn S.R., Oñate, E., Del Pin ,F., "The Particle Finite Element Method: a powerful tool to solve incompressible flows with free-surfaces and breaking waves". International Journal for Numerical Methods in Engineering 61, 2004, pp. 964-984.

Idelsohn S.R., Calvo, N., Oñate, E. "Polyhedrization of an arbitrary 3D point set". Computer Methods in Applied Mechanics and Engineering, 192, 2003, pp. 2649-2667

Idelsohn, S.R., Oñate, E., Calvo, N., Del Pin, F., "The meshless finite element method". Int. J. Numer. Methods Engrg., 58(6), 2003, pp. 893-912

Kara, F., Vassalos, D., "Hydroelastic analysis of cantilever plate in time domain", Ocean Engineering, Vol. 34, 1, 2007, pp. 122-132.

Lamb, H., "Hydrodynamics", Cambridge University Press, 1932.

Larese, A., Rossi, R., Oñate, E., Idelsohn, S.R., "Validation of the Particle Finite Element Method (PFEM) for Simulation of Free surface Flows". International Journal of Computational Methods. Accepted for publication.

Liang, C., Liao ,C., Tai, Y., Lai, W., "The free vibration analysis of submerged cantilever plates", Ocean Engineering, Vol. 28, 9, 2001, pp. 1225-1245.

Lindholm, U.S., Kana,D.D., Chu,W.H., Abramson, H.N., "Elastic Vibration Characteristics of Cantilever Plates in Water", Journal of Ship Research, Vol. 9, 1, 1965, pp. 11-22.

Oñate, E., "A stabilized finite element method for incompressible viscous flows using a finite increment calculus formulation". Computer Methods in Applied Mechanics and Engineering, 182, 2000, pp. 355-370

Oñate, E., Idelsohn, S.R., "A mesh free finite point

method for advective diffusive transport and fluid flow problems´´. Computational Mechanics, 21, 1998, pp. 283-292

Oñate, E., Idelsohn, S.R., Del Pin, F., Aubry, R. "The Particle Finite Element Method. An overview´´. International Journal of Computational Methods, 2, 2004, pp. 267-307

Osher, S., Fedkiw, R.P., (2006) Level Set Methods an dynamic implicit surfaces. Springer, 2006

Osher, S., Fedkiw, R.P. (2001) "Level Set Methods: An Overview and some recent results". Journal of Computational Physics 169, 2001, pp. 463-502.

Rognebakke, O., Hoff, J.R., Allers, J., Berget, K., Berge, B.O., Zhao, R., "Experimental approaches for determining sloshing laods in LNG tanks", Proc. Soc. of Naval Architects and Marine Engineers (SNAME) Annual meeting, Houston, 2005, pp. 1-15.

Roubtsova, V., Kahawita, R. "The SPH technique applied to free-surface flows". Computers and Fluids, 35, 2006, pp. 1359-1371.

Souto-Iglesias, A., Delorme, L., Pérez-Rojas, L., Abril-Pérez, S., "Liquid moment amplitude assessment in sloshing type problems with Smooth Particle Hydrodynamics", Ocean Engineering, 33, 2006, pp. 1462-1484.

Volterra, E., Zachmanoglou, E.C., Dynamics of vibrations, Charles E. Merrill, 1965.

Walhorn, E., Kölke, A., Hübner, B., Dinkler, D., "Fluid-structure coupling within a monolithic model involving free surface flows", Computers & Structures, 83, 25-26, 2005, pp. 2100-2111.

Zienkiewicz, O.C., Taylor, R.L., Nitharasu, P., The finite element method. Fluid dynamics, Elsevier, Vol. III, 2005.